Progress In Electromagnetics Research C, Vol. 76, 119–127, 2017

Wide-Angle Polarization Independent Triple Band Absorber Based on Metamaterial Structure for Microwave Frequency Applications

Khusboo Kumari, Naveen Mishra, and Raghvendra Kumar Chaudhary*

Abstract—This paper presents a wide-angle polarization independent triple-band absorber based on a metamaterial structure for microwave frequency applications. The designed absorber structure is the combination of two resonators (resonator-I and resonator-II). The proposed absorber is ultra-thin in thickness ($0.012\lambda_o$ at lowest resonance frequency and $0.027\lambda_o$ at highest resonance frequency). The proposed absorber structure offers three absorption bands with peak absorptivities of 99.95%, 95.32% and 99.47% at 4.48, 5.34 and 10.43 GHz, respectively. Additionally, it also offers the full width at half maximum (FWHM) bandwidth of 167.2 MHz (4.40–4.56 GHz), 178.1 MHz (5.25–5.43 GHz) and 393.8 MHz (10.24–10.63 GHz), respectively. The metamaterial property of the designed absorber structure has been discussed by using dispersion diagram plot. The designed absorber structure exhibits wide-angle absorption at various oblique incidence angle for both TM and TE polarizations. The absorption mechanism of the designed absorber structure has been analyzed through electric field and surface current distribution plots. The input impedance of the designed absorber (375.67 Ω at 4.48 GHz and 346.73 Ω at 10.43 GHz) nearly matches the free space impedance. The proposed absorber structure is fabricated and measured. Simulated and measured results are in good agreement with each other.

1. INTRODUCTION

Electromagnetic metamaterials (MTMs) [1] have gained significant advantages in the field of microwave engineering due to their unique properties of negative refractive index [2] and simultaneous negative values of permeability and permittivity [3]. In 1967, a Russian physicist Victor Vesselago theoretically illustrated the concepts of MTM [1] and discussed the formation of left-handed triad through the propagation of electromagnetic waves with the phase constant, electric and magnetic field vectors. After being inspired by Pendry et al.'s work [4, 5], Shelby et al. [6] experimentally illustrated the first left-handed MTM in 2001 at microwave frequency regime. In last few years, MTM has been used in various electromagnetic applications, such as antenna [7], cloaking [8], filter [9] and absorber [10, 11]. Nowadays, MTM based absorbers have been discussed due to their advantages of ultra-thin thickness, near unity absorption and many more, over conventional absorbers. MTM absorbers are usually composed of metal-dielectric-metal layers. The top metallic layer contains periodic arrangement of resonators. In order to restrict the transmission of electromagnetic waves, the complete copper backing has been done with the bottom metallic layer. Many MTM absorber structures have been reported for single-band [12, 13], dual-band [14], broadband [15] and triple-band [16, 17] applications. Article [18] studies a single-band ultra-compact MTM absorber, which consists of a three-dimensional square frame designed on the top of a metal backed FR4 substrate. Article [13] discusses another single-band polarization insensitive metamaterial absorber, which is designed for X-band applications. In article [14], a dual-band MTM absorber with two scales of Jerusalem resonators is presented. Article [15] demonstrates a multi-layered

Received 17 May 2017, Accepted 21 July 2017, Scheduled 1 August 2017

* Corresponding author: Raghvendra Kumar Chaudhary (raghvendra.chaudhary@gmail.com).
The authors are with the Department of Electronics Engineering, Indian Institute of Technology (Indian School of Mines), Dhanbad, Dhanbad-826004, India.

metal-dielectric pyramidal structure and shows ultra-broadband polarization independent absorptivity. In Article [16], a novel triple-band polarization insensitive metamaterial absorber constructed with a periodic array of a new resonant structure is explained. A metallic planar spiral structure based triple band absorber is presented in [17].

This work discusses a wide-angle polarization independent triple-band absorber based on a metamaterial structure. The combination of two resonators (resonator-I and resonator-II) are responsible for the appearance of three absorption peaks. The corresponding three absorption peaks are 99.95% at 4.48 GHz, 95.32% at 5.34 GHz and 99.47% at 10.43 GHz. The designed absorber structure is polarization independent and ultra-thin ($0.012\lambda_o$ at the lowest resonance frequency and $0.027\lambda_o$ at the highest resonance frequency) in thickness. The absorptivity of the designed absorber structure is studied under various oblique incidence angles, where a high absorption of greater than 80% is observed for incident angle up to 60° for both TM and TE polarizations. Further, MTM property of the designed absorber is confirmed by using a dispersion diagram plot. The absorption behavior of the designed absorber is explained by using electric field distribution, surface current distribution and input impedance plot.

2. DESIGN OF PROPOSED UNIT CELL

The arrangement of the designed absorber unit cell along with wave propagation direction and incident electric and magnetic field direction is shown in Fig. 1. The top layer of the designed unit cell is composed of two resonators (resonator-I and resonator-II) which are imprinted on the top of an FR-4 epoxy dielectric substrate ($\varepsilon_r = 4.4$, $\tan\delta = 0.02$) having thickness of 0.8 mm. Copper ($\sigma = 5.8 \times 10^7$ s/m) is present on both sides of the substrate having thickness 0.035 mm. The geometrical proportions of the designed unit cell of Fig. 1 are in mm as $L = 8.6$, $P = 8.2$, $P_1 = 5.575$, $A = 0.4$, $A_1 = 0.4$, $A_2 = 0.4$, $B = 1.825$, $C = 1.526$, $D = 1.5$, $G = 0.7$, $G_1 = 0.3$, $S = 0.3$, $S_1 = 0.3$, $R = 0.8$.

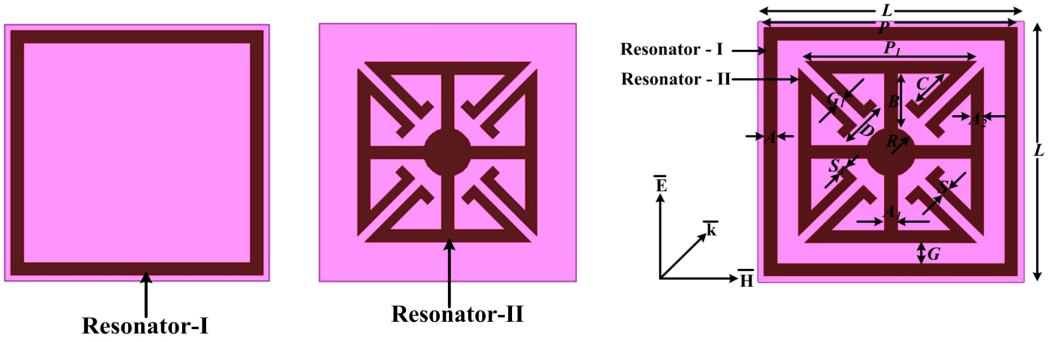

Figure 1. Top view of the proposed metamaterial absorber unit cell.

3. SIMULATION RESULTS

The proposed unit cell is simulated using ANSYS HFSS simulation software with master/slave periodic boundary conditions and Floquet port excitation. The absorptivity of the proposed structure can be calculated using Eq. (1),

$$A(\omega) = 1 - |S_{11}(\omega)|^2 - |S_{21}(\omega)|^2 \tag{1}$$

where $A(\omega)$, $|S_{11}(\omega)|^2$, and $|S_{21}(\omega)|^2$ denote absorbed power, reflected power and transmitted power, respectively. Due to full copper grounded on the bottom layer of the proposed structure, transmitted power can be reduced to zero, and hence Eq. (1) becomes,

$$A(\omega) = 1 - |S_{11}(\omega)|^2 \tag{2}$$

Hence, by reducing reflected power near unity absorption is achieved. The absorption curve, shown in Fig. 2(a), depicts comparison between absorptivitis of resonator-II and sub-resonator-II. It

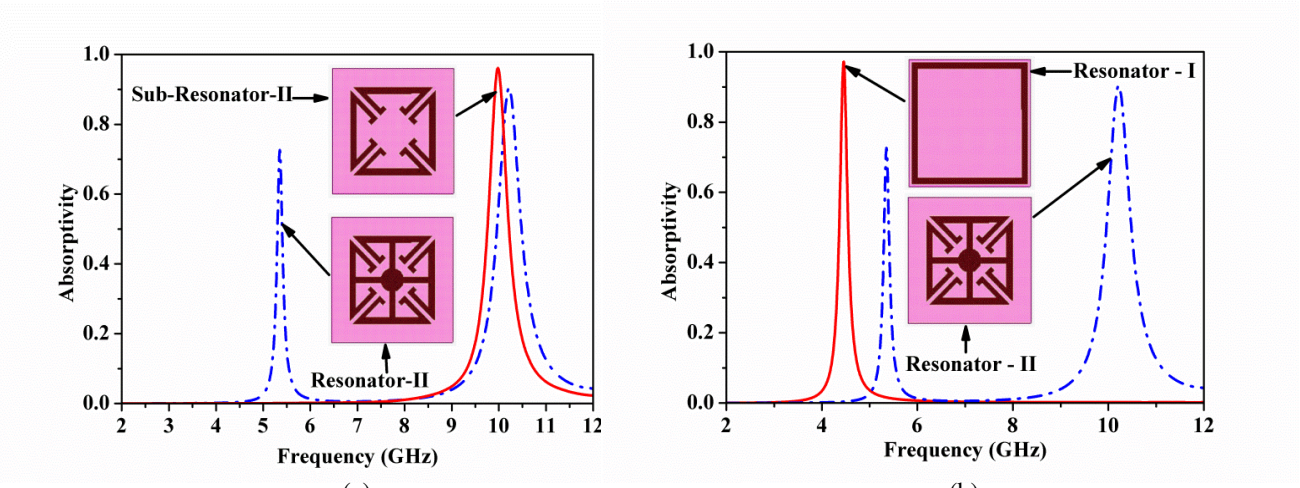

Figure 2. (a) Comparison between absorptivity curve for resonator-II and sub-resonator-II. (b) Absorptivity curve for resonator-I and resonator-II separately.

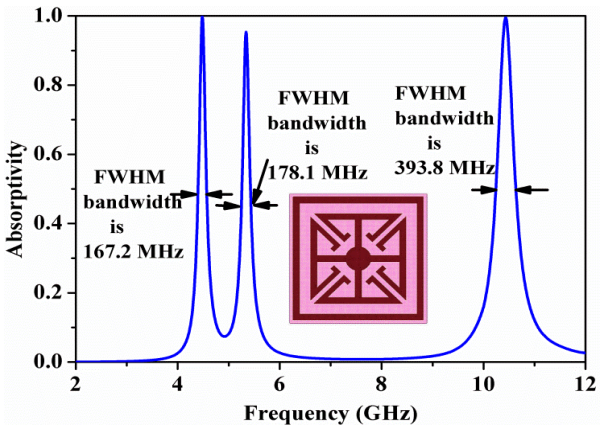

Figure 3. Simulated Absorption curve for the proposed metamaterial absorber structure.

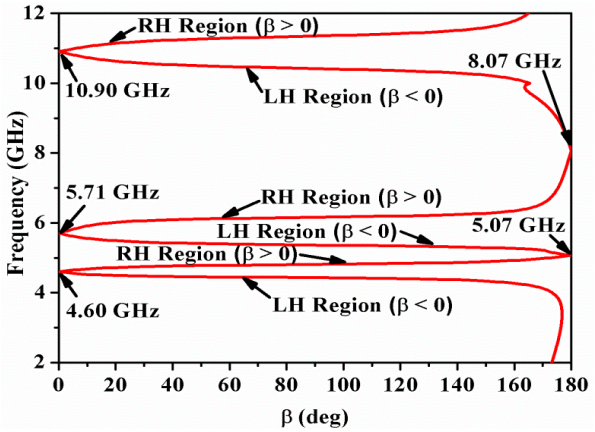

Figure 4. Dispersion diagram plot for the proposed metamaterial absorber structure.

is observed that resonator-II is responsible for the occurrence of dual bands with peak absorption value of 72.64% at 5.35 GHz and 90.39% at 10.21 GHz while the sub-resonator-II generates single band with peak absorption value of 96.10% at 9.98 GHz. The absorption curves for resonator-I and resonator-II are separately shown in Fig. 2(b). It describes that resonator-I is responsible for the origination of single band with peak absorption value of 97.20% (4.46 GHz), whereas remaining two absorption bands are due to resonator-II. The combination of these two resonators results in a triple-band absorber, as shown in Fig. 3. The three absorption bands occur at frequencies of 4.48 GHz (99.95%), 5.34 GHz (95.32%) and 10.43 GHz (99.47%) with FWHM bandwidths of 167.2 MHz (4.40–4.56 GHz), 178.1 MHz (5.25–5.43 GHz) and 393.8 MHz (10.24–10.63 GHz), respectively. In order to verify the metamaterial property for the designed absorber structure, dispersion diagram is plotted in Fig. 4. Further, the dispersion diagram plot is divided into left-handed (LH) region ($\beta < 0$), where propagation constant is positive, and right-handed (RH) region ($\beta > 0$), where propagation constant is negative. It is observed that all the three absorption bands of the designed absorber structure lie in LH region, which confirms the metamaterial property.

The designed structure is examined for various polarization angles (0° to 90° of steps size 15°). It is seen from Fig. 5 that due to four-fold symmetry, the peak absorptivity of the proposed absorber

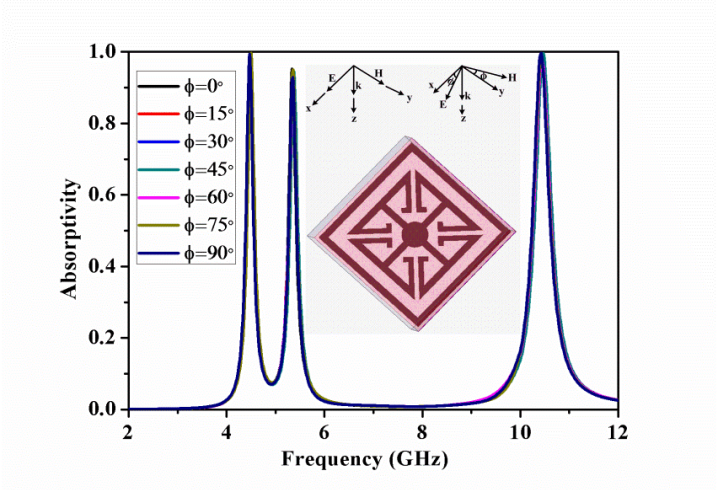

Figure 5. Absorption curve for proposed structure at varying polarization angles.

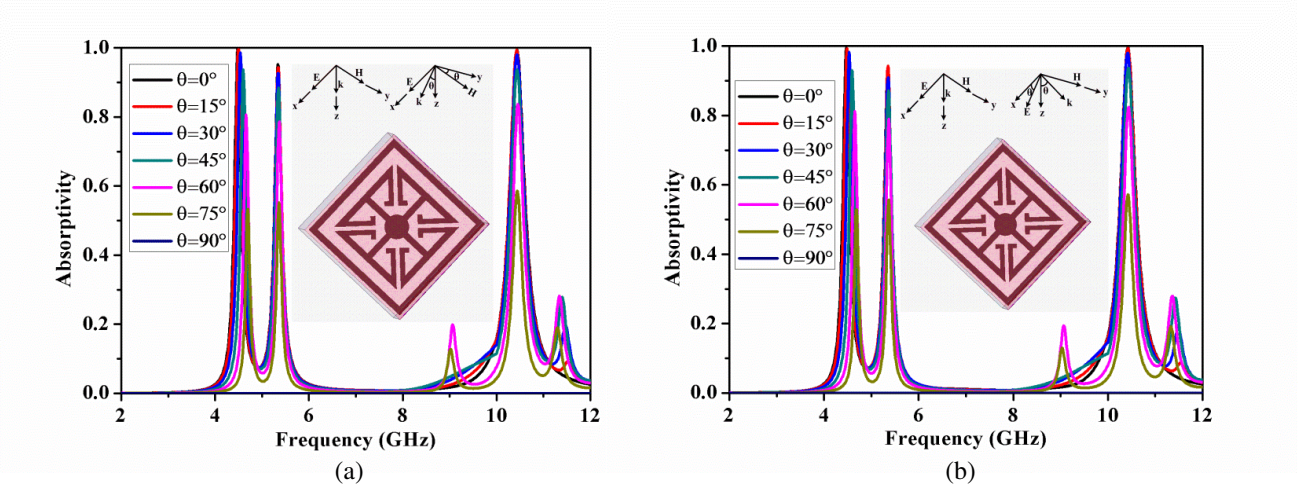

Figure 6. Absorption curve for proposed structure at different oblique incidence angles. (a) TE polarization. (b) TM Polarization.

structure remains the same for different polarization angles, which confirms polarization independent characteristics. Further, the structure is analyzed for various oblique incidence angle (0° to 90° in steps of 15°) for both TE and TM polarizations as shown in Fig. 6(a) and Fig. 6(b), respectively.

In the case of TE polarization, electric field direction is kept stable while magnetic field and wave vector direction are shifted for oblique incidence. In the case of TM polarization, magnetic field direction is kept stable while electric field and wave vector direction are shifted for oblique incidence. It is seen that by increasing incident angles, the absorptivity starts decreasing; however, a high absorption (more than 80%) is achieved up to 60° incidence angle for both TE and TM polarizations. This proves wide-angle absorption behavior of the proposed structure. The variation in incidence angle corresponds to generation of some small absorption peaks on both sides of the highest absorption peak of 10.43 GHz.

Electric field distribution plot for the designed absorber structure is shown in Fig. 7 which suggests that lower absorption peak at 4.48 GHz is controlled by resonator-I while the two higher absorption peaks at 5.34 GHz and 10.43 GHz can be controlled by left and right portions of resonator-II and top and bottom portions of resonator-II respectively.

Figure 8 shows surface current distribution plot on both layers of designed absorber unit cell at all the three absorption frequencies. It is seen that at 4.48 GHz, high concentration of surface current is mainly distributed in resonator-I. At 5.34 GHz, surface current mainly flows in the strip connecting left

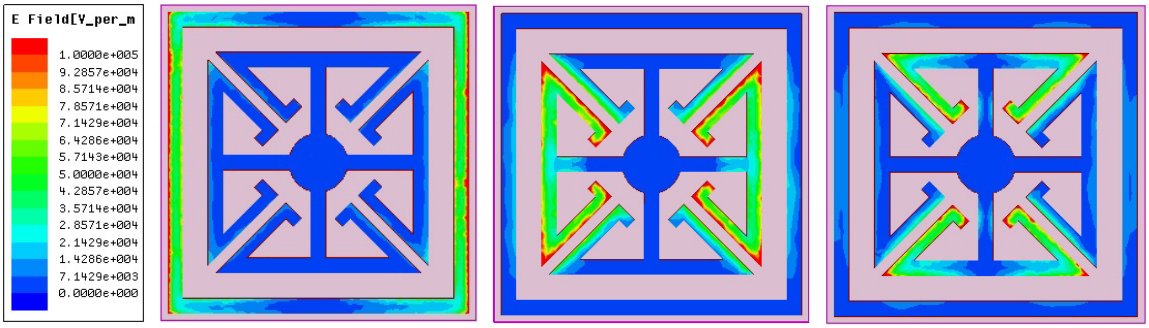

Figure 7. Electric field distribution plot for proposed absorber structure. (a) at 4.48 GHz, (b) at 5.34 GHz, (c) at 10.43 GHz.

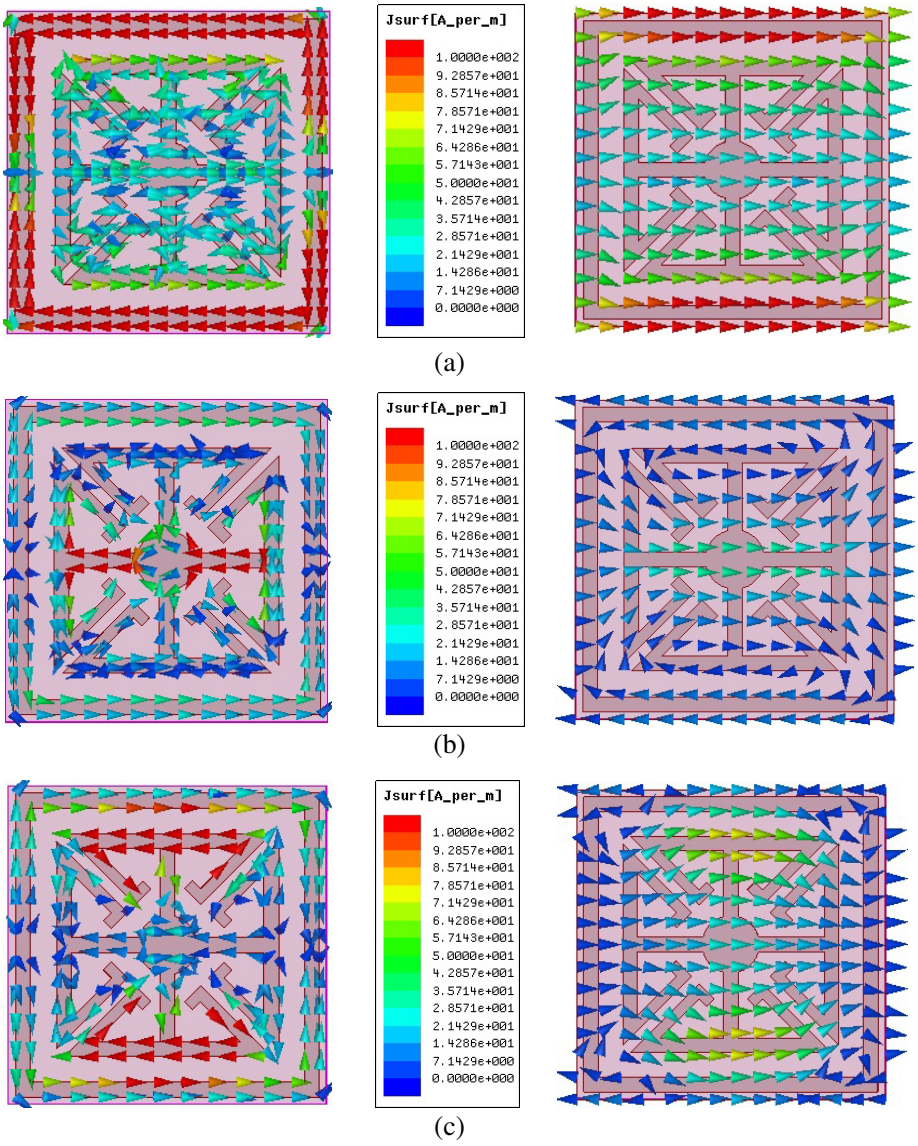

Figure 8. Surface current distribution plot at the top and bottom layer for the proposed absorber structure. (a) at 4.48 GHz, (b) at 5.34 GHz, (c) at 10.43 GHz.

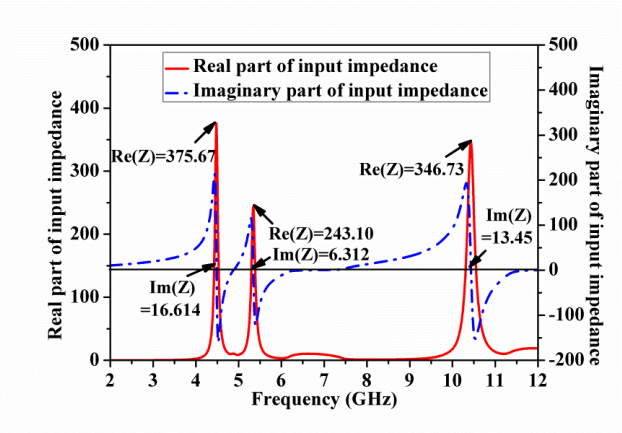

Figure 9. Input impedance plot for the proposed absorber structure.

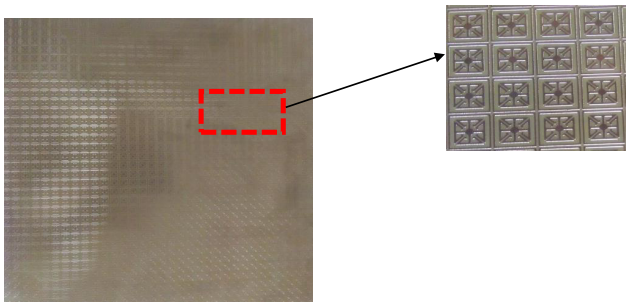

Figure 10. Fabricated prototype of the designed absorber structure.

and right portions of resonator-II while at 10.43 GHz, surface current is distributed at top and bottom portions of resonator-II. It is observed that the directions of surface current on both the metallic layers (top and bottom) at all the three absorption frequencies are anti-parallel to each other, constituting a circulating current loop in the direction perpendicular to the incident magnetic field, resulting in magnetic excitation. On the other hand, electric excitation occurs due to incident electric field at the top layer of the proposed structure as discussed in Fig. 7. Both electric and magnetic excitations take place at the resonant frequencies, resulting in high absorption of electromagnetic wave. Fig. 9 shows the input impedance plot for the designed absorber structure. It is observed that real and imaginary values of input impedance at 4.48 GHz and 10.43 GHz closely match free space impedance value of $377 + j0\Omega$, hence a high absorption is achieved. However, at 5.34 GHz real part of input impedance is far away from free space input impedance, hence a lower absorption peak is achieved. The real and imaginary parts of input impedance are obtained from Eq. (3) [18],

$$Z(\omega) = \eta_0 \sqrt{\frac{(1+S_{11})^2 - S_{21}^2}{(1-S_{11})^2 - S_{21}^2}} = \eta_0 \frac{1+S_{11}}{1-S_{11}} \tag{3}$$

Here, $Z(\omega)$ and η_0 denote input impedance and free space impedance, respectively.

Table 1 shows the values of real and imaginary parts of input impedance at all the three absorption frequencies.

Table 1. Real and imaginary part of input impedance at all the three absorption frequencies for the proposed structure.

Resonant Frequency (GHz) (fr)	**Real part of input impedance (Re(Z))**	**Imaginary part of input impedance (Im(Z))**	**Free space impedance (η_0 (in ohm))**
4.48	375.67	16.614	$377 + j0$
5.34	243.10	6.312	
10.43	346.73	13.45	

4. EXPERIMENTAL RESULTS

The designed absorber structure is fabricated on a $293 \times 293 \times 0.8$ mm^3 planar sheet of an FR-4 substrate, shown in Fig. 10. The measurement setup requires a fabricated structure and a separate pair of horn antennas connected to a network analyzer (Agilent N5221A PNA) each for X and C frequency band

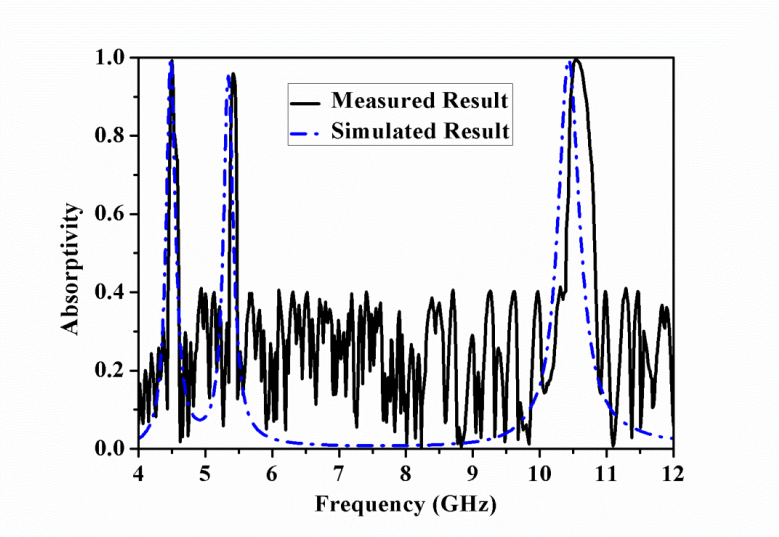

Figure 11. Measured and simulated absorptivity curves for the proposed absorber structure.

measurement, where one horn antenna is used for transmission of electromagnetic waves and the second horn used for reception purpose. Initially, reflection coefficient (S_{11} in dB) for copper metal plate is measured. After that, reflection coefficient (S_{11} in dB) for the fabricated structure is measured. The actual value of the reflection coefficient for the fabricated structure can be determined by normalizing the reflection coefficient of structure with the reflection coefficient of the copper metal plate. Finally, the absorptivity can be determined from the actual value of reflection coefficient. Fig. 11 shows the measured and simulated absorptivity curves for the proposed absorber structure. It is observed that both the results matches well with slight deviation in frequency, which may be due to fabrication and free space measurement imperfection.

The characteristics of the designed absorber are compared with previously published articles and shown in Table 2. The proposed absorber structure offers the least thickness among all the articles shown in table. In addition to above, the designed absorber offers more compactness than the previously published articles.

Table 2. Comparison of the proposed work with the earlier published ultrathin absorbers.

Parameters	**This work**	**[12]**	**[13]**	**[15]**	**[16]**
Lowest Absorption Peak (GHz)	4.48	8.65	5.95	3.07	9.86
Unit Cell Size (mm^3)	8.6 × 8.6 × 0.8	7 × 7 × 0.7	18.4 × 18.4 × 0.8	18 × 18 × 1.5	– ×–× 0.8
Ultrathin Thickness Corresponds to Lowest Absorption Peak (λ_0)	0.0119	0.0201	0.0158	0.0153	0.0263
Absorption Bands	Three	One	Two	Three	Three

5. CONCLUSION

The designed resonator for the proposed absorber structure is composed of two resonators (resonator-I and resonator-II). The combination of the two resonators is responsible for the occurrence of three absorption peaks with peak absorptive values of 99.95% at 4.48 GHz, 95.32% at 5.34 GHz and 99.47% at 10.43 GHz. The proposed structure is investigated under various oblique incidence angles, and a high absorption peak of greater than 80% is observed for incidence angle up to 60° for both TE and TM

polarizations. MTM property of the designed structure is explained by the dispersion diagram plot. Electric field distribution, surface current distribution and input impedance plot are used to explain the absorption behavior of the designed absorber structure. The proposed structure is ultra-thin in thickness ($0.012\lambda_o$) with respect to the lowest resonance frequency and ($0.027\lambda_o$) with respect to the highest resonance frequency.

ACKNOWLEDGMENT

This research work is supported by Science and Engineering Research Board (SERB), Department of Science & Technology (DST), Government of India, India under Project No. EMR/2016/002559.

REFERENCES

1. Caloz, C. and T. Itoh, *Electromagnetic: Transmission Line Theory and Microwave Applications*, John Wiley & Sons, Inc., 2006.
2. Shelby, R. A., D. R. Smith, and S. Schultz, "Experimental verification of a negative index of refraction," *Science*, Vol. 292, 77–79, 2001.
3. Veselago, V. G., "The Electrodynamics of substances with simultaneously negative values of ε and μ," *Soviet Physics Uspekh Usp. Fiz. Nauk*, Vol. 92, 509–514, 1964.
4. Pendry, J. B., A. J. Holden, D. J. Robbins, and W. J. Stewart, "Magnetism from conductors and enhanced nonlinear phenomena," *IEEE Trans. Microwave Theory Tech.*, Vol. 47, 2075–2081, 1999.
5. Pendry, J. B., A. J. Holden, D. J. Robbins, and W. J. Stewart, "Low-frequency plasmons in thin wire structures," *J. Physics, Condensed Matter*, Vol. 10, 4785–4809, 1998.
6. Shelby, R. A., D. R. Smith, and S. Schultz, "Experimental verification of a negative index of refraction," *Science*, Vol. 292, 77–79, 2011.
7. Mishra, N. and R. K. Chaudhary, "A miniaturized ZOR antenna with enhanced bandwidth for WiMAX applications," *Microwave and Optical Technology Lett.*, Vol. 58, 71–75, 2016.
8. Bilotti, F., S. Tricarico, and L. Vegni, "Plasmonic metamaterial cloaking at optical frequencies," *IEEE Transactions on Nanotechnology*, Vol. 9, 55–61, 2010.
9. Fouad, M. A. and M. A. Abdalla, "New π-T generalised metamaterial negative refractive index transmission line for a compact coplanar waveguide triple band pass filter applications," *IET Microw. Antennas Propag.*, Vol. 8, 1097–1104, 2014.
10. Li, H., L. H. Yuan, B. Zhou, X. P. Shen, Q. Cheng, and T. J. Cui, "Ultrathin multiband gigahertz metamaterial absorbers", *J. Appl. Phys.*, Vol. 110, 014909, 2011.
11. Landy, N. I., S. Sajuyigbe, J. J. Mock, D. R. Smith, and W. J. Padilla, "Perfect metamaterial absorber," *Phys. Rev. Lett.*, Vol. 100, 207402, 2008.
12. Lin, B.-Q., S.-H. Zhao, X.-Y. Da, Y.-W. Fang, J.-J. Ma, W. Li, and Z. H. Zhu, "Design of an ultracompact metamaterial absorber," *Microwave and Optical Technology Lett.*, Vol. 57, 1439–1441, 2015.
13. Thummaluru, S. R., N. Mishra, and R. K. Chaudhary, "Design and analysis of an ultra-thin X-band polarization — insensitive metamaterial absorber," *Microwave Optical Technology Lett.*, Vol. 58, 2481–2485, 2016.
14. Zhai, H., Z. Li, L. Li, and C. Liang, "A dual-band wide-angle polarization-insensitive ultrathin gigahertz metamaterial absorber," *Microwave and Optical Technology Lett.*, Vol. 55, 1606–1609, 2013.
15. Ding, F., Y. Cui, X. Ge, Y. Jin, and S. He, "Ultra-broadband microwave metamaterial absorber," *Applied Physics Letters*, Vol. 100, 103506, 2012.
16. Bian, B., S. Liu, S. Wang, X. K. Kong, H. Zhang, B. Ma, and H. Yang, "Novel triple-band polarization-insensitive wide-angle ultra-thin microwave metamaterial absorber," *Journal of Applied Physics*, Vol. 114, 194511, 2013.

17. Huang, X., H. Yang, S. Yu, J. Wang, M. Li, and Q. Ye, "Triple-band polarization-insensitive wide-angle ultra-thin planar spiral metamaterial absorber," *Journal of Applied Physics*, Vol. 113, 213516, 2013.
18. Smith, D. R., D. C. Vier, T. Koschny, and C. M. Soukoulis, "Electromagnetic parameter retrieval from inhomogeneous metamaterials," *Physics Review E*, Vol. 71, 036617, 2005.